Int. J. Electrochem. Sci., 8 **(2013)** 10280 - 10292

International Journal of
ELECTROCHEMICAL
SCIENCE
www.electrochemsci.org

Fabrication of Crack-Free Metal-Semiconductor-Metal Ultraviolet Photodetectors on Si (111) Substrates Based on Novel AlN/AlGaN Buffer Multilayer Scheme

Sheng-Po Chang

Institute of Microelectronics, Department of Electrical Engineering, and Advanced Optoelectronic Technology Center, National Cheng Kung University, Tainan 70101, Taiwan
E-mail: changsp@mail.ncku.edu.tw

Received: 3 June 2013 / *Accepted:* 29 June 2013 / *Published:* 1 August 2013

The GaN ultraviolet metal-semiconductor-metal (MSM) photodetectors epitaxially grown on Si (111) and sapphire (0001) substrates were prepared and characterized. By implementing our elaborate AlN/AlGaN buffer multilayer scheme on Si, the maximum responsivity of n^--GaN MSM photodetector with TiW transparent electrodes achieved at an incident wavelength of 359 nm was 0.187 A/W, which corresponds to the quantum efficiency of 64.7%. Furthermore, for a given bandwidth of 1 kHz and a given bias of 5 V, the corresponding noise equivalent power (NEP) of aforementioned photodetector was 1.53×10^{-12} W, which translates to a maximal detectivity (D^*) of 1.31×10^{12} cm-Hz$^{0.5}$W^{-1}.

Keywords: Gallium nitride (GaN), silicon (Si), sapphire, buffer multilayer, metal semiconductor-metal (MSM), ultraviolet photodetectors

1. INTRODUCTION

One of very important device applications for III-nitride semiconductors undoubtedly would be the area of photo-detection. In fact, because of their direct wide band-gap (E_g = 3.4 eV) and high saturation velocity ($v_s = 2.7\times10^7$ cm/sec), GaN and its associated compounds are widely considered as one of the most promising materials for the fabrication of ultraviolet (UV) photodetectors (PDs) [1-13]. The high performance UV PDs are vitally important for both civil and military applications including solar UV monitoring, source calibration, UV astronomy, flame sensors, detection of missile plumes, and securing space-to-space communications. The remarkable tolerability of III-nitrides to withstand aggressive environments is directly related to their thermal stability and radiation hardness.

Traditionally, GaN-based epitaxial layers were grown either on sapphire or on SiC substrates. Unfortunately, there are certain drawbacks associated with these substrates. For instance, sapphire is an insulator which has poor thermal conductivity. On the other hand, SiC substrate stands out in terms of thermal and electrical considerations, but it is deemed too expensive for popular use. Compared with sapphire and SiC substrates, GaN epitaxy on Si appears to be a compromising and cost effective solution. Another potential advantage of using Si substrate is the possibility of monolithically integrating GaN-based devices with Si-based microelectronics. Even though it is rather difficult to grow high quality GaN epitaxial layers on Si, however, GaN-based light emitting diodes and heterostructure field effect transistors prepared on Si substrates were still being successfully demonstrated [14-19]. We have previously reported the growth of high quality InGaN/GaN light-emitting diode (LED) epi-layers on Si (111) substrate [20]. We were able to grow high quality InGaN/GaN films on silicon substrate by incorporating an initial AlGaN buffer and two high-temperature (HT) AlN interlayers to effectively confine threading dislocation near the interfaces of AlGaN/HT-AlN buffer layers. In fact, our previous transmission electron microscopy (TEM) and scanning electron microscopy (SEM) studies confirmed the realizations of a smooth and crack-free GaN surface and a noticeable reduction in threading dislocation density away from the silicon substrate [20]. In this study, the growth of n^--GaN epitaxial layers on Si and sapphire substrates and the subsequent fabrication of GaN metal-semiconductor-metal (MSM) PDs on these substrates are discussed and compared. In particular, differences in the crystalline quality of epilayers, optical and electrical properties of fabricated PDs will be addressed.

2. EXPERIMENTS

Samples with three different epilayer structures (denoted as samples A, B, and C) used in this study were grown on Si (111) and sapphire (0001) substrates by metalorganic chemical vapor deposition (MOCVD) [21-24]. Trimethylgallium (TMGa), trimethylaluminium (TMAl) and ammonia (NH3) were used to supply the source materials for gallium (Ga), aluminium (Al) and nitrogen (N), respectively. Detailed growth procedures of these samples are outlined as follows:

2.1. Sample A: undoped GaN on Si with simple AlN/AlGaN buffer layers

After annealing Si substrate at 1100^{o}C in H_2 ambient to remove surface contamination, an AlN nucleation layer was first deposited on Si substrate. A 300-nm-thick AlGaN layer was thereafter deposited on top of the AlN nucleation layer to serve as strain relax layer. By using this strain relax layer, a thick GaN active layer could be achieved without cracking. Finally, a 1-μm-thick undoped GaN layer was then grown at 1100^{o}C, as shown in Figure 1(a).

2.2. Sample B: undoped GaN on Si with AlN/AlGaN buffer multilayer structure

This is a substantially improved version of an epi-structure implemented earlier on sample A. For the lightly Si-doped n-type GaN (n^--GaN) structure, 25-nm-thick AlN buffer layer was deposited

onto the Si (111) substrate at 1090°C. Then, two stacks of buffer multilayer were inserted between a 25-nm-thick AlN buffer layer and a topmost 500-nm-thick 1090°C-grown n^--GaN epitaxial layer. Each stack of buffer multilayer consists of a 30-nm-thick 540°C-grown AlN layer, a 50-nm-thick 1090°C-grown AlN layer, a 60-nm-thick 1090°C-grown $Al_{0.3}Ga_{0.7}N$ layer, a 40-nm-thick 1090°C-grown $Al_{0.2}Ga_{0.8}N$ layer, and a 100-nm-thick 1090°C-grown undoped-GaN layer. The schematic structure is depicted in Figure 1(b). Notice that the AlN nucleation layer used in this study is altogether consist of a 25-nm-thick AlN grown at 1100°C, a 30-nm-thick AlN grown at 550°C, and a 50-nm-thick AlN grown at 1100°C.

2.3. Sample C: undoped GaN on sapphire substrate with GaN buffer layer

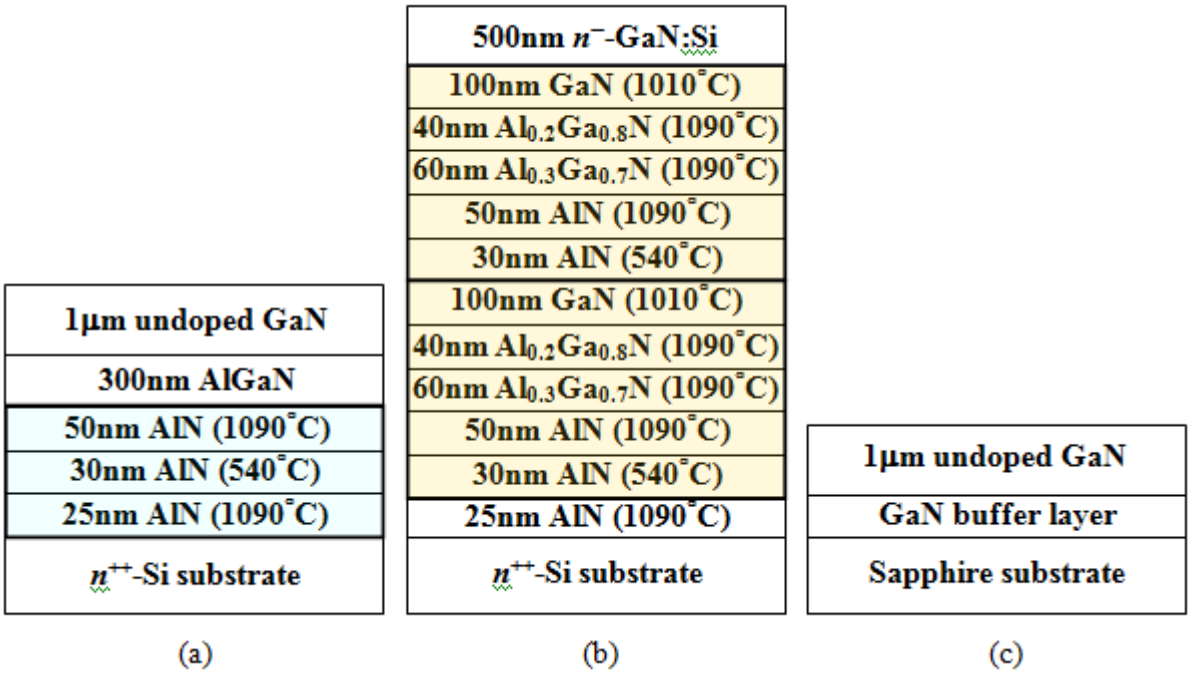

Figure 1. Schematics of GaN epilayer grown (a) on Si substrate coated with one set of AlN/AlGaN buffer layer, (b) on Si substrate coated with AlN/AlGaN buffer multilayer structure, and (c) on sapphire substrate with GaN buffer layer.

For comparison, a 1-μm-thick undoped GaN grown on sapphire substrate was also prepared, as shown in Figure 1(c). Once samples A through C were epitaxially prepared, MSM photodetectors were first fabricated by depositing Ni(4 nm)/Au(6 nm) semi-transparent contact layers on samples A and C using e-beam evaporator before conducting the furnace annealing at 500°C. Standard photolithography and lift-off were subsequently performed to fabricate interdigitated contact electrodes for MSM PDs. The Cr (40 nm)/Au (1000 nm) was then deposited and patterned as bonding pads. Each finger of Ni/Au contact electrodes was 7 μm wide, and with a spacing of 5 μm in between. The active area of fabricated PDs was 400×400 μm^2. As for MSM PDs on sample B, TiW (100 nm) and Ni (10 nm)/Au (90 nm) contact layers were then separately deposited onto the sample B using thermal evaporation

and RF magnetron sputter systems. Then, n⁻-GaN MSM photodetectors were thereafter fabricated by standard photolithography and lift-off process. The dimensions of each electrode finger of interdigitated metal contact fabricated on MSM photodetectors were 10 μm wide and 200 μm long, and with a gap of 10 μm in between. An HP-4156 semiconductor parameter analyzer was then used to measure dark current-voltage (I-V) characteristics of PDs on samples A, B, and C. Spectral responsivity measurements were also performed using JOBIN-YVON SPEX System equipped with a 450W xenon arc lamp light source and a standard synchronous detection scheme. Furthermore, the noise characteristics of fabricated GaN MSM UV PDs within a frequency range of 1 Hz to 1.6 KHz were measured using a low-noise current pre-amplifier and a dynamic signal analyzer.

3. RESULTS AND DISCUSSION

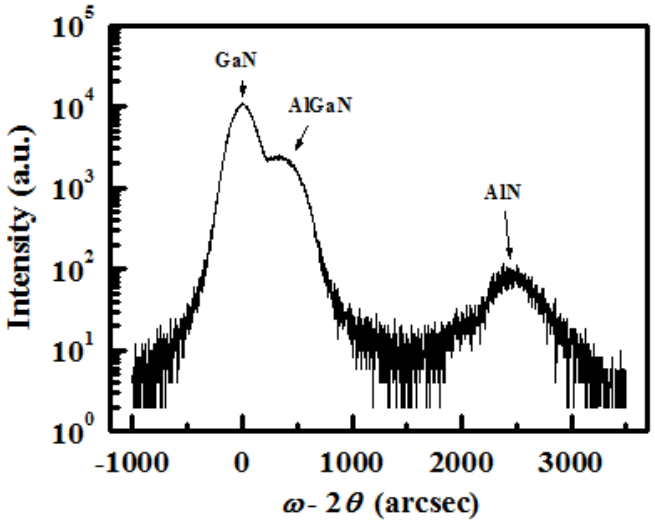

Figure 2. The DC-XRD analysis of n⁻-GaN epitaxial structure grown on silicon substrate.

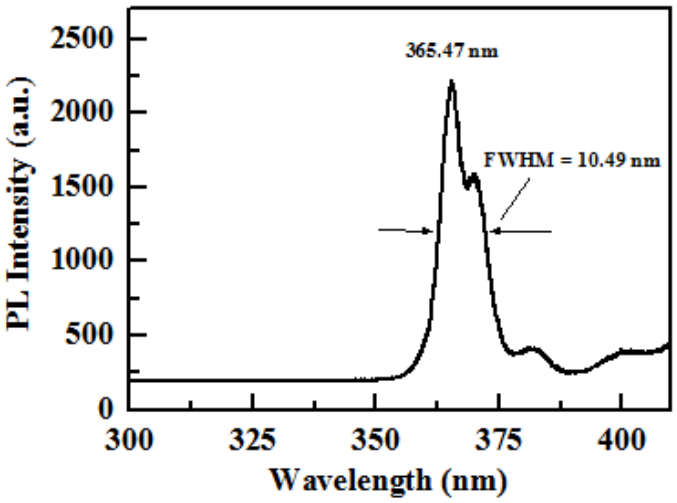

Figure 3. The photoluminescence (PL) analysis of n⁻-GaN epitaxial structure grown on silicon substrate.

Since sample B is a growth-refined version of epi-structure grown on silicon, We first conducted the x-ray diffraction and photoluminescence (PL) analyses on this very sample. Figure 2 shows the (002) Bragg reflection double-crystal X-ray diffraction (DCXRD) spectra of 500nm n^{-}-GaN epitaxial layer prepared on Si substrate. The full-width at half maximum (FWHM) of n^{-}-GaN epitaxial layer measured was 232.11 arcsec. Figure 3 presents the photoluminescence (PL) spectrum of 500nm n^{-}-GaN epitaxial layer grown on Si substrate. According to the PL spectrum, the highest spectral peak intensity of n^{-}-GaN epitaxial layer occurs at ~365.47 nm and the full-width at half maximum (FWHM) determined was 10.49nm (96.2meV).

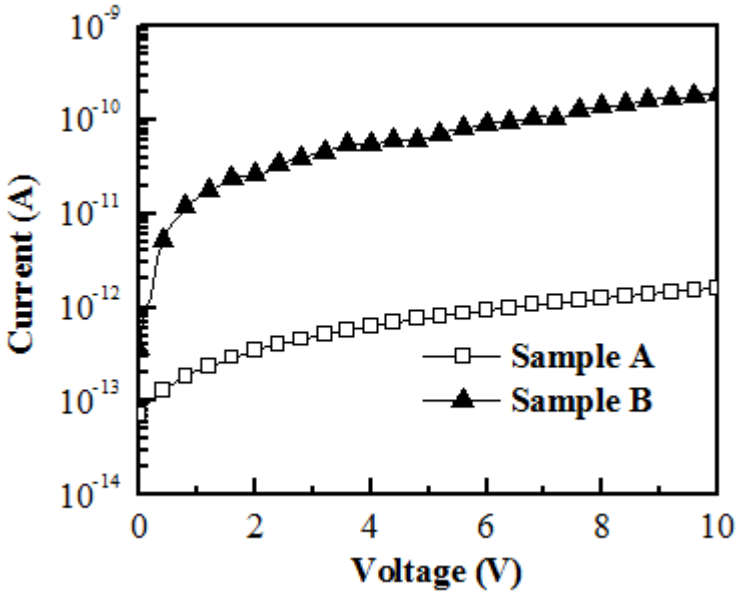

Figure 4. Measured dark I-V characteristics of MSM PDs fabricated on samples A (on Si) and C (on sapphire).

Figure 4 shows the measured dark I-V characteristics of MSM PDs fabricated on samples A (on Si) and C (on sapphire). With 5 V applied bias, the dark current of PDs on sample A was 7.8×10^{-13} A, which was about two orders of magnitudes lower than that of PDs on sample C. The result shown in Figure 4 was a bit of counter-intuitive since the defect density of GaN epitaxial layer grown on Si substrate was expected to be much higher than that of similar GaN structure grown on sapphire substrate. In other words, the highly compensated nature (due to charged defects) of samples A should exhibit characteristics of low electron mobility and high resistivity. To explain this anomalous phenomenon, the carrier transport in sample A believably could be dominated by hopping conduction within the bandgap and thereby being scattered by charged defects. Therefore, when compared with that of PDs on sample C (on sapphire), a much lower dark current was obtained from devices fabricated on samples A. The MSM photodetectors with different contact electrodes (TiW and Ni/Au) were also constructed on sample B (on Si with novel AlN/AlGaN buffer multilayer scheme).

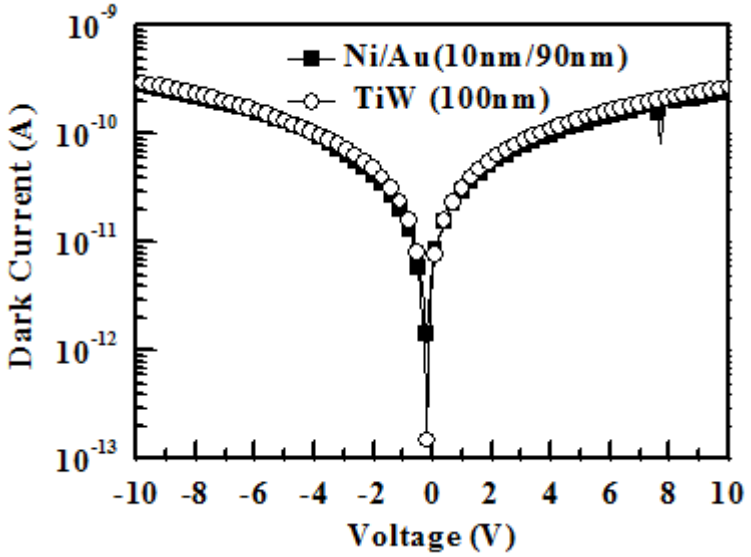

Figure 5. Dark I–V characteristics of the photodetectors with TiW and Ni/Au contact electrodes.

Figure 5 presents the symmetric I–V characteristics of MSM photodetectors with TiW and Ni/Au contact electrodes. Within a dark environment when 5V applied bias was administered, the resultant dark current of photodetectors with TiW and Ni/Au electrodes were 1.36×10^{-10} and 1.21×10^{-10} A, respectively.

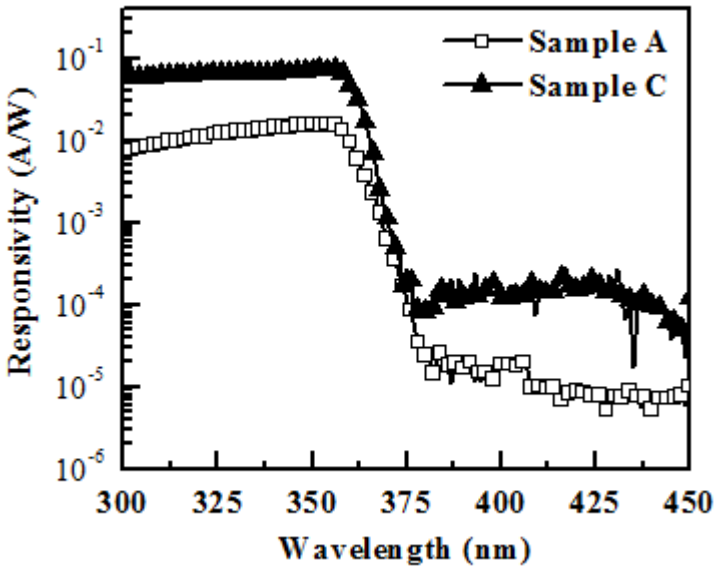

Figure 6. Room temperature spectral responses of MSM PDs fabricated on samples A and C with 5 V applied bias.

Notice that a relatively small dark leakage current could still be detected from our detectors covered with TiW or Ni/Au interdigitated finger electrodes, even though these III-nitrides based device

layers were grown on the lattice-mismatched silicon substrate. A small dark current obtained in our experiment clearly benefits from an insertion of two extra stacks of buffer multilayer into the device structure. This scheme undoubtedly helps to alleviate the impact of lattice-mismatch between GaN and silicon imposed on the epitaxial growth by further improving the crystalline quality of GaN films when the numbers of possible dislocations and defects are effectively minimized [26]. As of a result, a larger Schottky barrier height was obtained between contact electrode and epitaxial film.

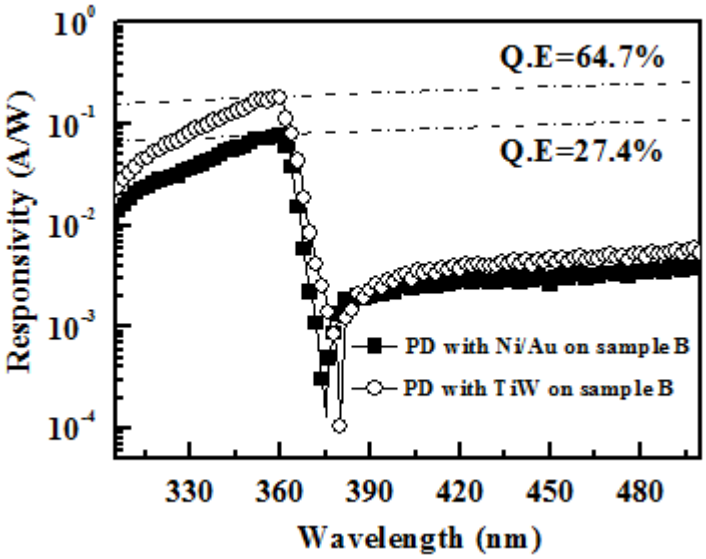

Figure 7. Spectral responses of fabricated detectors with TiW and Ni/Au electrodes determined with a 5V applied bias.

Next, both Figures 6 and 7 demonstrate room temperature spectral responses of MSM PDs on samples A, B, and C with 5 V applied bias administered. To quantify the peak responsivity, the xenon lamp intensity was first measured by a calibrated GaP UV detector, then the difference in sensor-detecting areas between GaP UV detector and our PDs was quantified in order to precisely estimate the PD responsivity. For PDs fabricated on samples A and C, Figure 6 clearly demonstrates the peak responsivity occurs at 355 nm for both MSM PDs. Numerically, the measured peak responsivities were 0.016 and 0.074 A/W for samples A and C, respectively. Compared with undoped GaN grown on sapphire substrate (i.e. sample C), a smaller peak responsivity observed from undoped GaN grown on Si substrate (i.e. sample A) was directly related to a highly defective epitaxial layer. Here, the rejection ratio is defined as the ratio between the responsivity measured at 355 nm and 425 nm. Therefore, rejection ratios as determined were 2100 and 420 for samples A and C, respectively. A much larger rejection ratio observed from sample A should be attributed to its lower dark current and thus a smaller responsivity detected in the below bandgap region. For comparison, similar measurements were also performed on devices with TiW and Ni/Au electrodes on sample B. The resultant peak responsivity was determined at 359 nm for both MSM PDs with different metal Schottky contacts. The maximum responsivities for MSM photodetectors with TiW and Ni/Au contact electrodes were 0.187 and 0.0792A/W, which corresponds to quantum efficiencies of 64.7 and 27.4%, respectively. In our case,

the responsivity is highly dependent on transmittance of contact electrode, so the higher transmittance of TiW renders a larger responsivity [26]. Below the cut off wavelength, the responsivity of both PDs appeared virtually similar, indicating a nearly identical schottky barrier height for TiW and Ni/Au contacts. In addition, we went a step further by defining the rejection ratio as the ratio between the spectral responsivity measured at 359 nm and 385 nm. The resultant rejection ratios were thereby determined as 111 and 43 for the MSM photodetectors with TiW and Ni/Au contact electrodes, respectively. A larger rejection ratio observed from the detector with TiW electrode was undoubtedly attributed to the higher transmittance of TiW electrode.

Figure 8 depicts the noise power spectra of two fabricated PDs (on sample A and C) with 5 V applied bias. The measured low frequency noises belonged to 1/f-type noise. Notice that sample A exhibits lower noise power density as compared to that of sample C, which again is related to its lower dark current.

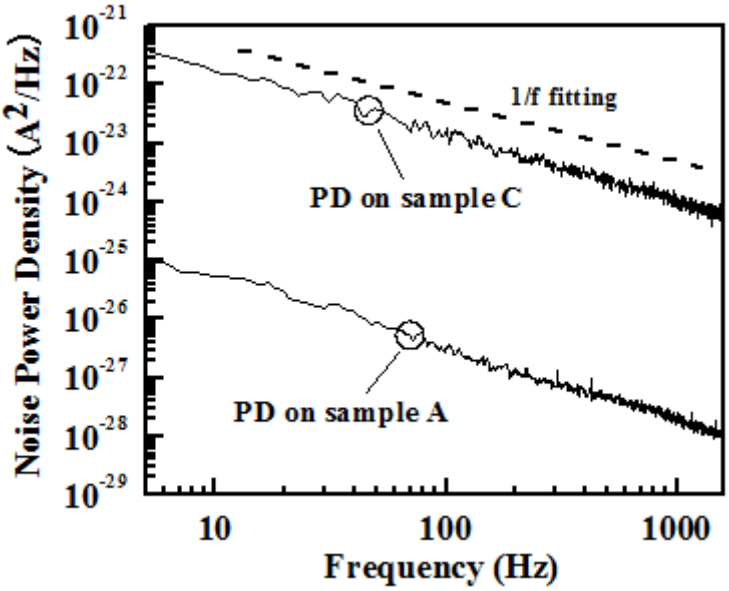

Figure 8. Noise power spectra of MSM UV PDs fabricated on samples A and C as determined with 5 V applied bias.

For comparison, Figures 9(a) and (b) show the measured noise power density of the GaN MSM photodetectors with Ni/Au and TiW contact electrodes, respectively. Noise curves indicate that 1/*f* (flicker) is a dominant noise mechanism, which is expected for MSM n^--GaN detectors operating at low frequency. Moreover, these noise curves satisfy the relation of Hooge-type equation with a fitting parameter α. Notice that the measured low frequency noise was classified as a 1/*f*-type ($\alpha = 1$) noise for low bias and a $1/f^2$-type ($\alpha = 2$) noise for high bias. Moreover, both Figures 10(a) and (b) depict the noise power density as a function of dark current measured at 100 Hz for the GaN MSM photodetectors with Ni/Au and TiW contact electrodes, respectively. We can derive the noise power density, S_n, using the Hooge-type equation:

$$S_n(f) \propto \frac{I^\beta}{f^\gamma}. \qquad (1)$$

From the curves shown in Figures 10(a) and (b), the β was around 1.07 at low bias and was elevated then to 4.3 at high bias for the photodetector with TiW contact electrode. On the other hand, the value of β found was around 1.16 at low bias and became 2.49 at high bias for the photodetector with Ni/Au contact electrode.

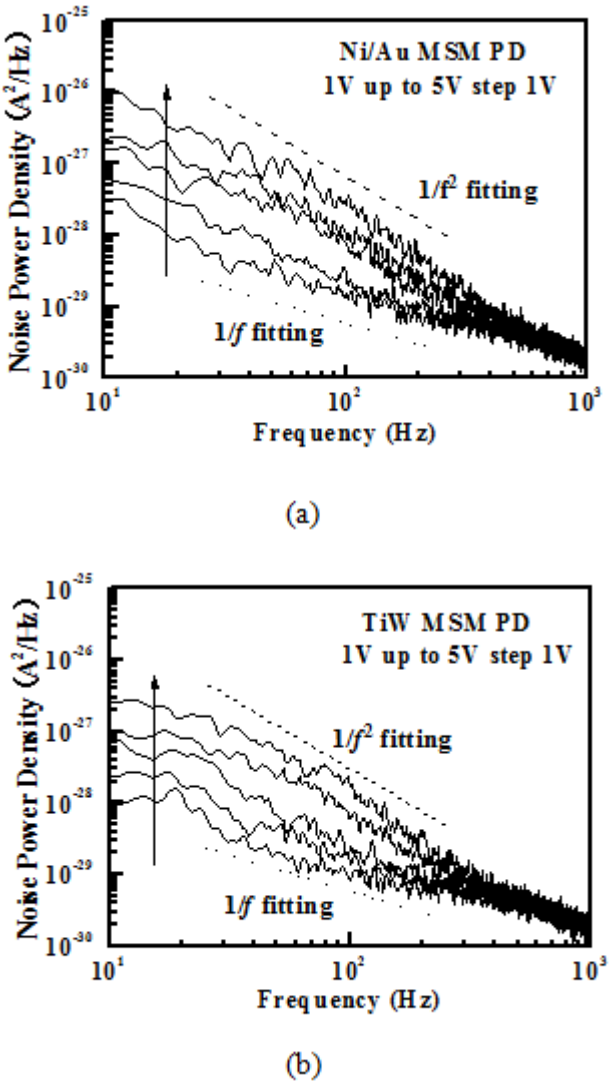

Figure 9. Measured noise power densities of the GaN MSM photodetectors fabricated on sample B with: (a) Ni/Au and (b) TiW contact electrodes.

The variance in the fitting parameter β extracted from PDs grown on Si substrate was attributed to the highly defective epitaxial layer. A large β again suggests some defect related states existed in the depletion region or in the forbidden gap of our photodetectors. These extra states contributed to a stronger trapping process, which was responsible for a larger noise observed. For a specified bandwidth (B), the total square of noise current, $\langle i_n \rangle^2$, can be determined by integrating the noise power density, $S_n(f)$,

$$\langle i_n \rangle^2 = \int S_n(f) df \ . \qquad (2)$$

On the other hand, noise equivalent power (*NEP*) can be calculated by

$$NEP = \sqrt{\frac{\langle i_n \rangle^2}{R}}, \quad (3)$$

where R is the responsivity of the PDs. With 5 V applied bias, the values of corresponding NEP as measured were 7.30×10^{-11} and 1.17×10^{-9} W for devices constructed on samples A and C, respectively.

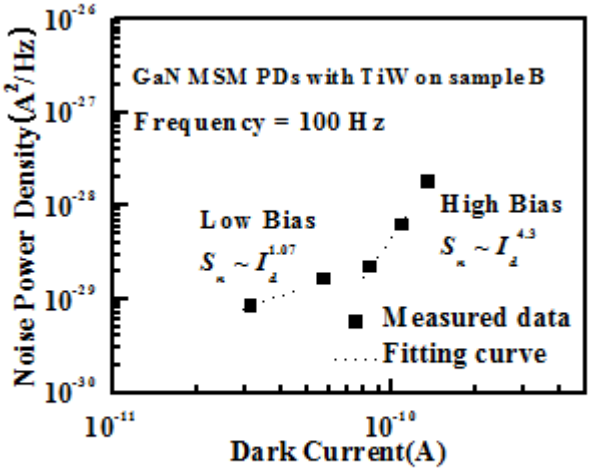

(a)

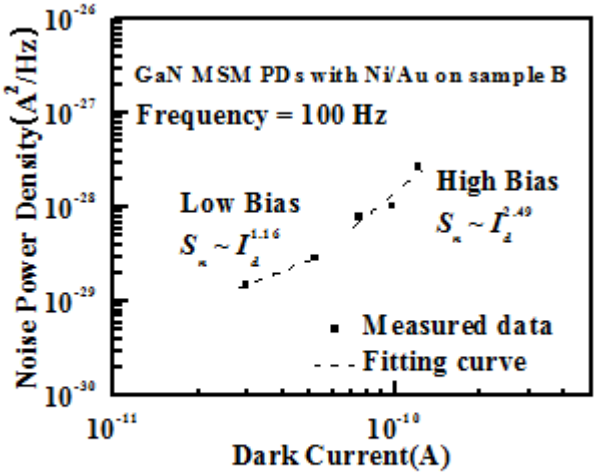

(b)

Figure 10. Noise power density as a function of dark current measured at 100 Hz for the GaN MSM photodetectors fabricated on sample B with: (a) TiW and (b) Ni/Au contact electrodes.

A smaller NEP observed from GaN PDs prepared on Si substrates should be attributed to the smaller noise power densities obtained, as shown in Figure 9. For comparison, for a given bandwidth of 1 kHz and a given bias of 5 V, the corresponding noise equivalent powers of our n^--GaN MSM

photodetectors with TiW and Ni/Au electrodes fabricated on sample B were 1.53×10^{-12} and 5.12×10^{-12} W, respectively. Furthermore, the normalized detectivity (D^*) can be determined by

$$D^* = \frac{\sqrt{A}\sqrt{B}}{NEP}, \quad (4)$$

where A is the area of the photodetector and B is the bandwidth. For PDs fabricated on samples A and C, with a given bandwidth of 1 kHz, a PD active area of $400\times400\ \mu m^2$, and a 5 V applies bias, the resultant values of D^* as measured were 1.73×10^{10} and 1.08×10^{9} cmHz$^{0.5}$W^{-1} for samples A and C, respectively. It should be noted that D^* determined from GaN MSM PD prepared on Si substrate was comparably larger than that of conventional GaN MSM PD prepared on sapphire substrate, which again was benefited directly by a smaller noise power density achieved for PD prepared on Si substrate.

Table I. The relative benchmark values of MSM photodetectors fabricated on Samples A, B, and C.

Measurement condition	MSM PDs on Sample A (on Si)	MSM PDs on Sample B (on Si with buffer multilayer)		MSM PDs on sample C (on sapphire)
		TiW	Ni/Au	
Dark current measured at 5V	7.8×10^{-13} A	1.36×10^{-10} A	1.21×10^{-10} A	6.46×10^{-11} A
Peak responsivity (R)	0.016 A/W (at λ_{peak} = 355 nm)	0.187 A/W (at λ_{peak} = 359 nm)	0.0792 A/W (at λ_{peak} = 359 nm)	0.074 A/W (at λ_{peak} = 355 nm)
Rejection ratio	R (355 nm)/R (425 nm) = 2100	R (359 nm)/R (385 nm) = 111	R (359 nm)/R (385 nm) = 43	R (355 nm)/R (425 nm) = 420
NEP measured at 5 V	7.30×10^{-11} W	1.53×10^{-12} W	5.12×10^{-12} W	1.17×10^{-9} W
Detectivity (D^*) at 5 V	1.73×10^{10} cm-Hz$^{0.5}$·W^{-1}	1.31×10^{12} cm-Hz$^{0.5}$·W^{-1}	3.91×10^{12} cm-Hz$^{0.5}$·W^{-1}	1.08×10^{9} cm-Hz$^{0.5}$·W^{-1}

However, photodetectors with a much better performance could be realized when sample B with a novel AlN/AlGaN buffer multilayer structure implemented on Si was adopted as a substrate. In fact, based on the aforementioned results, the corresponding detectivities (D^*) of 1.31×10^{12} and 3.91×10^{11} cm-Hz$^{0.5}$W^{-1}, respectively, were measured as result. Notice that these values of D^* were all comparably larger than those extracted from GaN MSM photodetectors fabricated on samples A (on Si) and C (on sapphire). A smaller noise power density of the PDs prepared on Si (111) substrate (sample B) is evidently benefited by the incorporation of an elaborate AlN/AlGaN buffer multilayer scheme. The relative benchmark values of MSM photodetectors fabricated on Samples A, B, and C are summarized in TABLE I for comparison. The experimental results obtained from photo-detection devices fabricated on (111) silicon demonstrate that our MSM photodetectors are well-suited for low-noise applications. Compared to the NEP and D* values reported for other PDs [27-28], those for Sample B is significantly better.

4. CONCLUSION

In summary, GaN ultraviolet MSM photodetectors grown and fabricated on Si (111) and sapphire (0001) substrates were prepared. With a novel AlN/AlGaN buffer multilayer scheme

implemented, the resultant dark current of PDs prepared on Si substrate with was much smaller than that of similar devices prepared also on silicon and sapphire substrates. In addition, with an incident wavelength of 359 nm, the maximum responsivity for the n^--GaN MSM photodetectors with TiW and Ni/Au contact electrodes fabricated on silicon coated with buffer multilayer was 0.187 and 0.0792A/W, corresponding to the quantum efficiency of 64.7 and 27.4%, respectively. Finally, for a given bandwidth of 1 kHz and a given bias of 5 V, the achieved lowest noise equivalent powers of our n^--GaN MSM photodetectors with TiW and Ni/Au electrodes were 1.525×10^{-12} and 5.119×10^{-12} W, respectively, which led to the detectivity (D^*) of 1.313×10^{12} and 3.914×10^{11} cm-$Hz^{0.5}W^{-1}$, respectively.

ACKNOWLEDGMENTS

The authors would like to thank the National Science Council and Bureau of Energy, Ministry of Economic Affairs of Taiwan, R.O.C., for the financial support under Contract No. 101-2221-E-006-139 and 101-D0204-6, and the LED Lighting Research Center of NCKU for the assistance of device characterization. This work was also supported in part by the Center for Frontier Materials and Micro/Nano Science and Technology, the National Cheng Kung University, Taiwan, as well as by the Advanced Optoelectronic Technology Center, the National Cheng Kung University, under projects from the Ministry of Education.

References

1. Y. Z. Chiou, Y. K. Su, S. J. Chang, J. Gong, Y. C. Lin, S. H. Liu, and C. S. Chang, *IEEE J. Quantum Electron.*, 39 (2003) 681.
2. E. Monroy, E. Muñoz, F. J. Sánchez, F. Calley, E. Calleja, B. Beaumont, P. Gibart, J. A. Muñoz, and F. Cussó, *Semicond. Sci. Technol.*, 13 (1998) 1042.
3. G. Y. Xu, A. Salvador, W. Kim, Z. Fan, C. Lu, H. Tang, H. Morkoç, G. Smith, M. Estes, B. Goldenberg, W. Yang, and S. Krishnankutty, *Appl. Phys. Lett.*, 71 (1997) 2154.
4. M. Mosca, J. L. Reverchon, N. Grandjean, and J. Y. Duboz, *IEEE J. Sel. Top. Quantum Electron.*, 10 (2004) 752.
5. N. Biyikli, I. Kimukin, O. Aytur, and E. Ozbay, *IEEE Photon. Technol. Lett.*, 16 (2004) 1718.
6. N. Biyikli, I. Kimukin, T. Tut, T. Kartaloglu, O. Aytur, and E. Ozbay, *Semicond. Sci. Technol.*, 19 (2004) 1259.
7. G. Parish, S. Keller, P. Kozodoy, J. P. Ibbetson, H. Marchand, P. T. Fini, S. B. Fleischer, S. P. DenBaars, U. K. Mishra, and E. J. Tarsa, *Appl. Phys. Lett.*, 75 (1999) 247.
8. A. Osinsky, S. Gangopadhyay, R. Gaska, B. Williams, M. A. Khan, D. Kuksenkov, and H. Temkin, *Appl. Phys. Lett.*, 71 (1997) 2334.
9. V. Adivarahan, G. Simin, J. W. Yang, A. Lunev, M. A. Khan, N. Pala, M. Shur, and R. Gaska, *Appl. Phys. Lett.*, 77 (2000) 863.
10. S. J. Chang, M. L. Lee, J. K. Sheu, W. C. Lai, Y. K. Su, C. S. Chang, C. J. Kao, G. C. Chi, and J. M. Tsai, *IEEE Electron. Dev. Lett.*, 24 (2003) 212.
11. O. Katz, V. Garber, B. Meyler, G. Bahir, and J. Salzman, *Appl. Phys. Lett.*, 79 (2001) 1417.
12. E. Monroy, T. Palacios, O. Hainaut, F. Omnès, F. Calle, and J. F. Hochedez, *Appl. Phys. Lett.*, 80 (2002) 3198.
13. J. L. Pau, C. Rivera, E. Muñoz, E. Calleja, U. Schühle, E. Frayssinet, B. Beaumont, J. P. Faurie, and P. Gibart, *J. Appl. Phys.*, 95 (2004) 8275.
14. C. F. Shih, N. C. Chen, C. A. Chang, and K. S. Liu, *Jpn. J. Appl. Phys.*, 44 (2005) L140.

15. H. Ishikawa, K. Asano, B. Zhang, T. Egawa, and T. Jimbo, *Physica Status Solidi A*, 201 (2004) 2653.
16. S. Iwakami, M. Yanagihara, O. Machida, E. Chino, N. Kaneko, H. Goto, and K. Ohtsuka, *Jpn. J. Appl. Phys.*, 43 (2004) L831.
17. A. Curutchet, N. Malbert, N. Labat, A. Touboul, C. Gaquiere, A. Minko, and M. Uren, *Microelectronics Reliab.*, 43 (2003) 1713.
18. P. Javorka, A. Alam, A. Marso, M. Wolter, J. Kuzmik, A. Fox, M. Heuken, and P. Kordos, *Microelectronics J.*, 34 (2003) 435.
19. V. Hoel, Y. Guhel, B. Boudart, C. Gaquiere, J. C. De Jaeger, H. Lahreche, and P. Gibart, *Electron. Lett.*, 37 (2001) 1095.
20. Y. P. Hsu, S. J. Chang, W. S. Chen, J. K. Sheu, J. Y. Chu, and C. T. Kuo, *J. Electrochem. Soc*. 154 (2007) H191.
21. S. J. Chang, W. C. Lai, Y. K. Su, J. F. Chen, C. H. Liu and U. H. Liaw, *IEEE J. Sel. Top. Quantum Electron.*, 8 (2002) 278.
22. S. J. Chang, C. S. Chang, Y. K. Su, R. W. Chuang, Y. C. Lin, S. C. Shei, H. M. Lo, H. Y. Lin and J. C. Ke, *IEEE J. Quan. Electron.*, 39 (2003) 1439.
23. S. J. Chang, C. H. Kuo, Y. K. Su, L. W. Wu, J. K. Sheu, T. C. Wen, W. C. Lai, J. F. Chen and J. M. Tsai, *IEEE J. Sel. Top. Quantum Electron*., 8 (2002) 744.
24. S. J. Chang, C. S. Chang, Y. K. Su, C. T. Lee, W. S. Chen, C. F. Shen, Y. P. Hsu, S. C. Shei and H. M. Lo, *IEEE Tran. Adv. Packaging*, 28 (2005) 273.
25. Yu-Zung Chiou, *IEEE Electron Device Lett.*, 26 (2005) 172.
26. C. K. Wang, S. J. Chang, Y. K. Su, Y. Z. Chiou, S. C. Chen, C. S. Chang, T. K. Lin, H. L. Liu, and J. J. Tang, *IEEE Trans. Electron Dev.*, 53 (2006) 38.
27. Y. Z. Chiou, *Semicond. Sci. Technol.*, 23 (2008) 125007.
28. S. P. Chang, S. J. Chang, Y. Z. Chiou, C. Y. Lu, T. K. Lin, Y. C. Lin, C. F. Kuo, and H. M. Chang, *J. Electrochem. Soc.*, 154 (2007) J209.